JOURNAL OF GEOPHYSICAL RESEARCH, VOL. 103, NO. C11, PAGES 24,781–24,797, OCTOBER 15, 1998

Statistical aspects of surface drifter observations of circulation in the Santa Barbara Channel

E. P. Dever, M. C. Hendershott, and C. D. Winant

Scripps Institution of Oceanography, University of California, San Diego, La Jolla

Abstract. Argos-tracked drifters are used to study the near-surface circulation in the Santa Barbara Channel. The mean consists of a cyclonic cell in the western Santa Barbara Channel with weaker flow in the eastern Channel. Drifter mean velocities agree well with record means from near-surface current meters. At the eastern entrance to the channel, drifter velocities are biased toward outflow (eastward velocity) conditions. Drifter variability at synoptic and seasonal scales shows a tendency for upwelling and eastward flow in spring, a strong cyclonic circulation in summer, poleward relaxation in fall, and weak, variable circulation in winter. Drifter estimates of eddy stress divergence indicate advective terms play a secondary role in the mean surface momentum balance. Lagrangian time and space scales are about 1 day and under 10 km, respectively. The mismatch between Lagrangian and Eulerian timescales indicates advective terms are important to the fluctuating circulation.

1. Introduction

The Santa Barbara Channel extends from Point Conception in the west to Port Hueneme in the east (Figure 1) with a string of four islands defining its southern, offshore boundary. The channel is approximately 100 km long and 50 km wide. It marks a region of transition and mixing between warmer, saline waters found in the Southern California Bight and colder, fresher waters upwelled to the north. This, in combination with the complicated local wind field, bathymetry, and lateral boundaries, makes the circulation complex and, until recently, not well understood [*Hendershott and Winant*, 1996].

The Santa Barbara Channel is the site of active oil and gas resource development, and concern regarding the consequences of this has motivated much of the research in the region. Circulation in the Santa Barbara Channel was first studied in detail in the wake of a 1968 oil spill. Using hydrographic surveys and drift cards, *Kolpack* [1971] described a counterclockwise mean circulation in the western channel and a northwesterly flow through the eastern part. Continuing concern about oil spill trajectories led the Minerals Management Service (MMS) to fund studies in 1983 and 1984 to provide information about the boundary conditions at the eastern and western entrances to the channel as well as the interisland passages [*Brink and Muench*, 1986; *Gunn et al.*, 1987; *Auad*, 1996; *Auad et al.*, 1998]. These studies reinforced an appreciation of the complicated nature of circulation within the channel. In particular channel circulation was not consistently correlated with the wind as is commonly the case on shelves with strong wind forcing [e.g., *Smith*, 1981; *Winant et al.*, 1987].

Other historical studies include the Organization of Persistent Upwelling Structures (OPUS) program [*Brink et al.*, 1984; *Atkinson et al.*, 1986; *Barth and Brink*, 1987] which focused on the northwestern channel region between Point Arguello and Point Conception. A major finding was that water upwelled near Point Conception could take a variety of paths to the south including paths leading into the channel. Speculations as to the causes of differing upwelling plume directions included channel outflow conditions and offshore eddies, but no definitive statements could be made. The same study also demonstrated the complicated spatial structure of the wind field near Point Conception [*Caldwell et al.*, 1986].

The knowledge gained during these studies reinforced an appreciation of the complexity and large variability of circulation on timescales up to several years within the Santa Barbara Channel. The present field program includes moorings within the interior of the Santa Barbara Channel, synoptic expendable bathythermograph (XBT), conductivity-temperature-depth (CTD), and acoustic Doppler current profiler (ADCP) cruises and meteorological stations [*Hendershott and Winant*, 1996]. An important part of this field program has been the deployment of Argos-tracked near-surface drifters over a 5-year period. This constitutes the first large-scale deployment of drifters throughout the Santa Barbara Channel. The relative uniformity of the drifter sampling and the availability of moored near-surface observations make possible statistical analyses of the

Paper number 98JC02403
0148-0227/98/98JC-02403$09.00

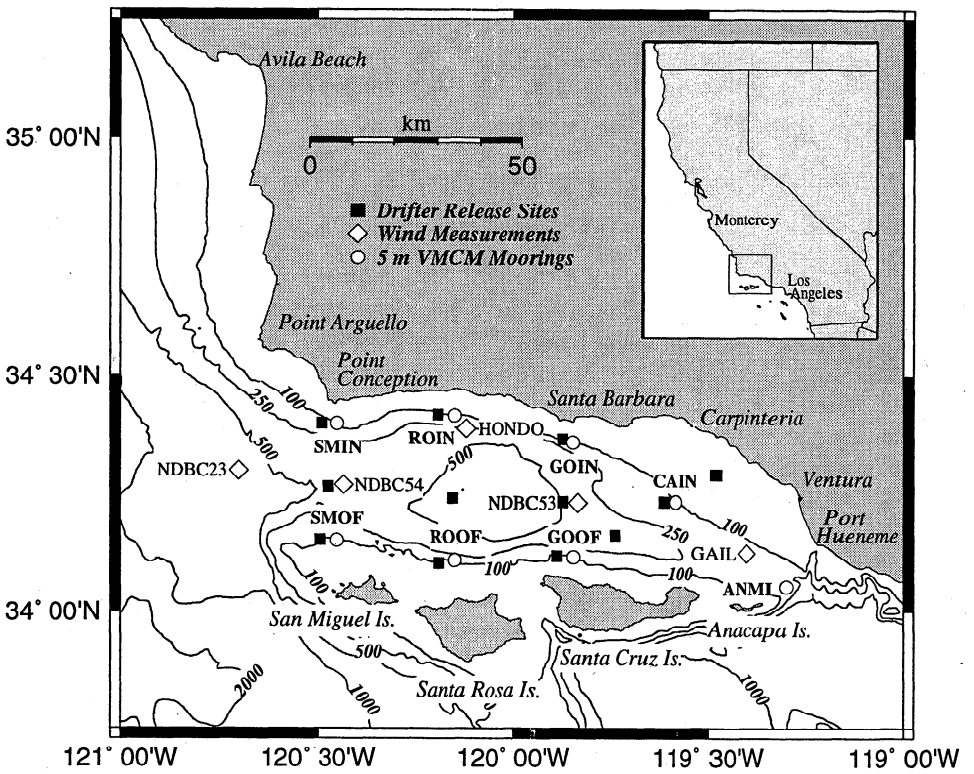

Figure 1. The Santa Barbara Channel, showing drifter deployment sites (solid squares), vector-measuring current meter (VMCM) moorings (open circles), and wind measurement locations (open diamonds). National Data Buoy Center (NDBC) numbers are abbreviated to their last two digits, e.g., NDBC23 corresponds to 46023. NDBC buoys also included downward looking acoustic Doppler current profilers (ADCPs) during some periods.

drifter data in addition to qualitative descriptions of drifter tracks.

The goals of this paper are to use statistical analyses of the drifter data in order to (1) improve our understanding of the mean near-surface circulation within the Santa Barbara Channel and the variability about that mean, (2) compare surface Lagrangian observations with near-surface Eulerian observations, (3) gain insight into the mean surface momentum balance within the channel, and (4) estimate Lagrangian time and space scales within the channel.

The remaining structure of the paper is as follows. In section 2, drifter sampling and data processing are described. Eulerian statistics of drifter data are presented in section 3. This includes a detailed comparison to near-surface current meter data. In section 4, the Eulerian averages of drifter data are used to estimate terms in the mean surface momentum balance. Lagrangian statistics of the flow within the channel are described in section 5. Results are summarized in section 6.

2. Data

2.1. Drifter and Sampling Program Designs

The surface drifters used here are very similar to the *Davis* [1985a] Coastal Ocean Dynamics Experient (CODE) design. A central cylindrical case houses batteries and electronics. Four nylon sails are attached with fiberglass rods. Spherical styrofoam floats tied to the ends of the rods provide buoyancy. The nominal sampling depth of the drifters is 0.5 m. The primary difference between these drifters and the CODE type is the use of Argos rather than radio tracking. Positions were acquired for at least 40 days. Generally, four to five fixes per day are available with an accuracy of under 1 km (most often, under 300 m). Drifters also measured temperature (calibrated to 0.01°C) once per minute and averaged them hourly.

Our data come almost entirely from drifters deployed on 23 occasions between May 1993 and November 1997. Additional data from a few drifters deployed in testing and for oil spill response drills are also used. To sample the seasonal variability, deployments were spaced about every 3 months. The drifter deployment positions (Figure 1) were spaced approximately uniformly within the channel. Generally, one drifter was released at each location, though on some occasions, a pair was released. In general, drifters released in the northwest channel exited within 3 to 4 days, while drifters released in the southern and eastern channel resided for 10 days or longer. About half of the drifters released within the southern and eastern channel beached within the channel. Analysis of moored observations within the Santa Barbara Channel [*Harms*, 1996; *Harms and Winant*,

1998] has shown that large-scale variability of the surface circulation can often be categorized as one of a number of synoptic patterns that persists for weeks. Because drifters usually exit the channel or beach within 10 days, each drifter deployment generally samples one synoptic state.

2.2. Data Processing

Interpretation of position data (particularly time differencing to obtain velocity estimates) within a coastal region presents complications as compared to the open ocean. Drifters that had clearly beached had their records truncated when they first reached their beaching position. However, some drifters approached the coast quite closely and remained there for several days, only to later return to the open channel. Whether these drifters had actually beached is an open question. However, they exhibited behavior quite different from drifters found in the open channel. Histograms of drifter speed as a function of distance from the coast showed little variation in speed distributions far from the coast. Within 1.5 km of the coast a rapid falloff in speeds occurred. Therefore drifter observations within 1.5 km of the coast were edited out.

Open ocean drifter observations are often treated with a low-pass filter to remove inertial oscillations. Because of the short spatial scales of the Santa Barbara Channel and the short residence time of many drifters within the channel, low pass filtering is not an option. Instead, position data are linearly interpolated onto a 6-hour time base that is near the mean time between fixes. Velocities were determined by finite differences of the interpolated positions. Data gaps longer than 12 hours and clearly erroneous fixes (over land, etc.) were removed from consideration. The use of 6 hour interpolated positions retains the maximum possible temporal resolution. However, motions with periods less than 12 hours are aliased, and tidal and inertial periods are marginally resolved. Fortunately, tidal and inertial oscillations do not dominate drifter velocity fluctuations within the Santa Barbara Channel as evidenced by the fact that Lagrangian autocorrelation functions (discussed in section 5) generally do not have significant peaks at tidal or inertial periods.

3. Eulerian Statistics

We present velocity statistics over 12.5 km by 12.5 km bins. The bin size is a compromise between the desire to maximize resolution and maintain statistical reliability. Drifter tracks in the Santa Barbara Channel make it obvious that a strong cyclonic circulation is often present in the western portion of the Santa Barbara Channel. Elsewhere, drifter trajectories indicate generally slower circulation over the mainland shelf between Santa Barbara and Port Hueneme and variable circulation north of Santa Cruz. A 12.5 km bin size resolves the western cyclonic circulation and the mean circulation in areas near the mainland, in the central channel, and along the channel islands. At least 49 (6 hourly) observations are present in each bin with a median number of 155 observations.

As *Davis* [1985b, 1991] and others [e.g., *Poulain et al.*, 1996; *Swenson and Niiler*, 1996] note, velocity statistics calculated from Lagrangian observations are subject to a number of biases. In particular, a bias is expected for velocities calculated outside a deployment region. Floats in these bins preferentially sample fluid parcels leaving the deployment region. The deployment locations here minimize this bias within most of the channel. However, the easternmost deployment locations ran between Santa Cruz Island and Carpinteria (Figure 1). This leaves the eastern entrance to the Santa Barbara Channel outside the deployment region and subject to array bias. We choose to present velocities calculated in the entire Santa Barbara Channel including the eastern entrance and extreme southern and western entrances with the understanding that statistics in these areas are biased toward outflow conditions.

Within the central Santa Barbara Channel, bias is minimized, but statistical uncertainty remains. *Davis* [1991] has derived several expressions for the variance of velocity about a mean derived from drifter observations. These expressions consider a set of progressively simplifying assumptions. His final expression includes the assumption that the averaging area is much larger than the spatial scales of the time and space covariance. This is appropriate when averaging areas are much larger than the dominant scales of flow as is typical in open ocean drifter velocity estimates. However, in the Santa Barbara Channel, our averaging areas are smaller than the scales of flow. *Davis'* [1991] variance estimate for arbitrary flow scales is

$$(\delta U_k)^2 = \int_L dt \int_L d\tilde{t} \int_A dx \int_A d\tilde{x}[E_{kk}(\mathbf{x}-\tilde{\mathbf{x}}, t-\tilde{t}) \times \sum_n \sum_m \langle \delta[\mathbf{x}-\mathbf{r}(t|n)]\delta[\tilde{\mathbf{x}}-\mathbf{r}(\tilde{t}|m)]\rangle]/(CAL)^2 \quad (1)$$

where $(\delta U_k)^2$ is the variance estimate for the mean U velocity component in the k direction, L is the length of time of the observations, n and m are indices for drifter observations, t and $\tilde{t}$ ($\mathbf{x}$ and $\tilde{\mathbf{x}}$) indicate times (positions) for the n and m drifter observations, A is the averaging area, E_{kk} is the time- and space-lagged covariance, δ signifies integration only over drifters in A at the appropriate time lag, and C is the mean number of drifters in area A over time L.

Use of (1) requires an estimate of E_{kk}. We estimate E_{kk} from the time-lagged Eulerian autocorrelation functions along principal axes. This is calculated from current meter records and scaled by the drifter velocity variances along principal axes. We then assume that within each bin, $E_{kk}(\mathbf{x}-\tilde{\mathbf{x}}, t-\tilde{t}) = E_{kk}(0, t-\tilde{t})$, i.e., perfect spatial covariance within A. For each bin the nearest current meters (Figure 1) are used. Typical (one sided) Eulerian decorrelation times are 5 to 7 days (Figure 2). Therefore observations within 5–7 days of

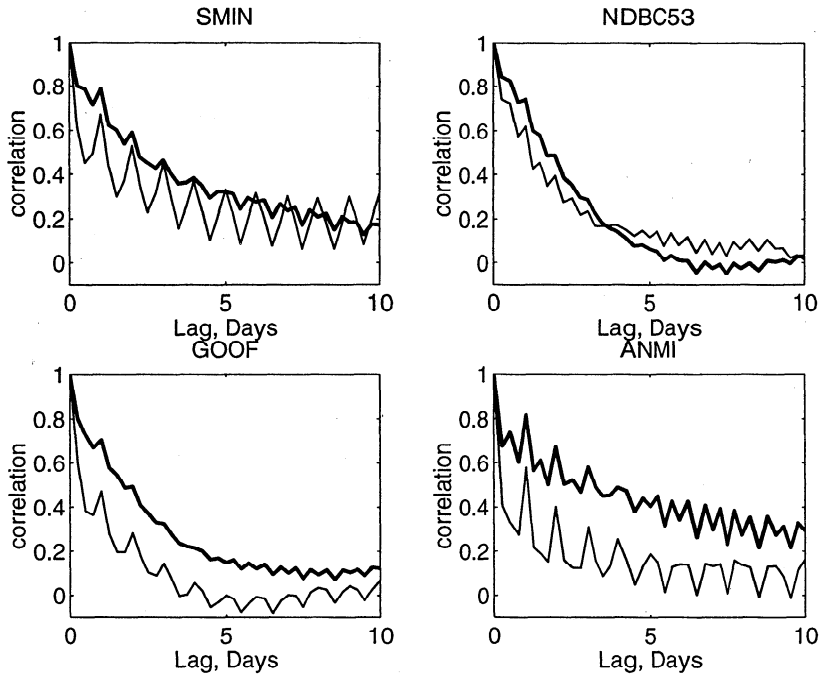

Figure 2. Representative autocorrelation functions along principal axes estimated from current meters. For consistency with drifter velocity estimates, 6-hour averaged data were used. The major axis autocorrelation function is indicated by the thick line, while the minor axis autocorrelation function is shown by the thin line. Current meters are VMCMs at 5 m, except at NDBC buoys, where ADCP bins at 24 m were used. ADCP autocorrelations are believed to be representative of those at 5 m, as *Harms* [1996] found strong correlations between VMCMs at 5 and 45 m.

each other reduce δU_k less than those widely separated in time (i.e., from different deployments).

The assumption of perfect spatial covariance within a bin is conservative in that the true spatial covariance is imperfect and instrumental errors on drifter velocities are independent. However, the decorrelation times discussed above are dominated by synoptic variability and do not represent seasonal variability.

3.1. Means and Principal Axes

Throughout the rest of this paper we use the term mean without modifiers to describe the long-term average of the circulation over several years, whether it is estimated from pseudo-Eulerian averages over all drifter deployments or record averages of moored observations. Other types of averages, such as seasonal averages, averages over individual deployments, or Lagrangian averages over the displacements of a single drifter, are specified as such.

The mean near-surface velocities averaged over 12.5 km by 12.5 km bins are presented in Figure 3. The means and standard deviations along principal axes (Figure 3b) show a strong mean cyclonic circulation in the western Santa Barbara Channel with a weaker mean circulation in the eastern Santa Barbara Channel. Standard deviations are generally aligned with the mean flow. They are most strongly polarized near the mainland and channel island coasts with little polarization in the center. For comparison, record average 5 m vector-measuring current meter (VMCM) velocities and standard deviations (for 6-hour block-averaged velocities) are also shown. The uncertainties about the drifter means estimated from (1) are shown in Figure 3c. Over most of the channel, the agreement is quite good in the magnitudes and directions of the means and standard deviations. An exception occurs in the eastern Santa Barbara Channel where drifters have preferentially sampled outflow conditions. This occurs where bins are outside the region of drifter deployment (Figure 1). However, the mean eastward flow in the southeast Santa Barbara Channel is not entirely due to a bias. A mean eastward velocity exists at least as far as Santa Cruz Island as indicated by the mean VMCM velocity there. Bins along the extreme western and southern boundaries of the channel outside the deployment area may also be somewhat biased toward outflow conditions.

In comparing the drifter and VMCM velocities, there are also differences in detail. The magnitudes of mean drifter velocity vectors, as well as principal axes, are generally about 20% larger than those of the 5 m VMCM data. Differences in direction are also evident near the CAIN mooring north of the eastern end of Santa Cruz. Possible explanations for this type of drifter and VMCM velocity disagreement include biased sampling on the

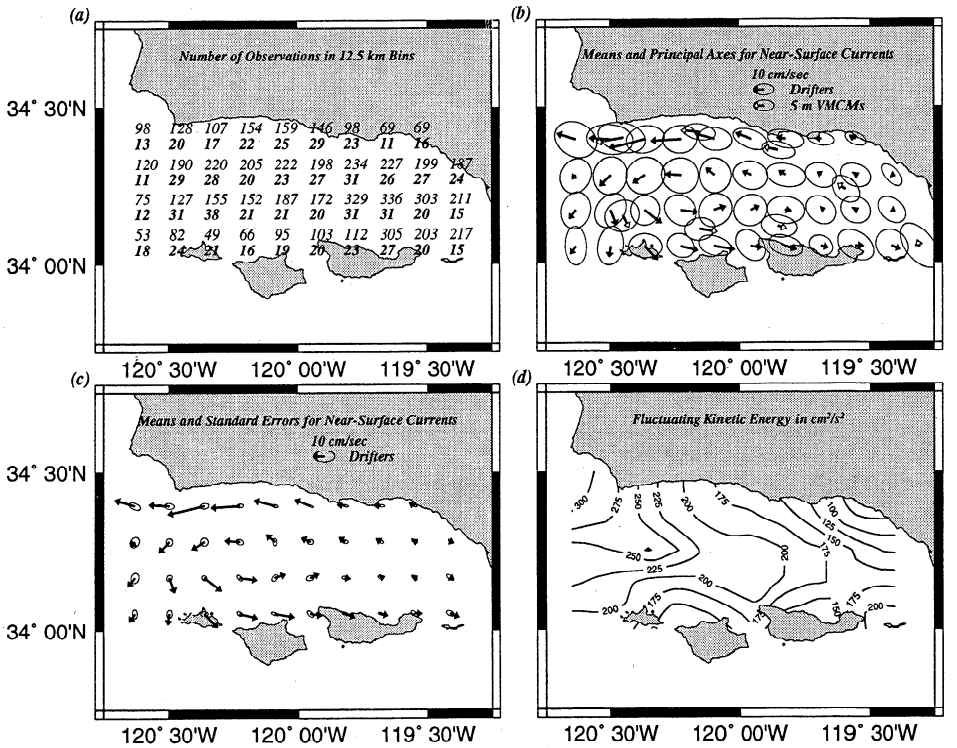

Figure 3. Drifter velocity statistics over 12.5 km by 12.5 km bins. (a) Total (italic) and effectively independent (bold italic) numbers of 0.25-day drifter observations in each bin. (b) Means and standard deviations along principal axes for drifters (solid arrows) and 5-m VMCMs (open arrows). (c) Drifter means with standard error estimates. These are much smaller than means, except in the southeast channel. (d) Fluctuating kinetic energy scaled by density. The fluctuating kinetic energy includes all timescales of fluctuations from seasonal to inertial and tidal.

part of drifters, near-surface velocity shear, instrumental error on the part of either the drifters or current meters, Stokes drift, and small-scale spatial variability.

Contours of fluctuating kinetic energy make clear regions of flow variability. The highest-amplitude fluctuations are near the western entrance. Fluctuations are highest here because rapidly moving drifters may either exit the channel through the western entrance or remain in the channel and recirculate in the western cyclonic cell. Fluctuating kinetic energies are also large northeast of Santa Rosa Island. This is probably associated with the Santa Rosa cold squirt, a mushroom-shaped plume of cold water frequently extending from Santa Rosa toward Santa Barbara [*Hendershott and Winant*, 1996]. This feature, often evident in satellite sea surface temperature images, carries drifters northeastward away from Santa Rosa Island. Lowest values of fluctuating kinetic energy exist over the relatively broad northeastern shelf between Port Hueneme and Santa Barbara and north of Santa Cruz Island.

Standard errors are largest where means and fluctuations are largest, i.e., the western cyclonic cell (Figure 3c). However, in this region, means are much larger than standard errors. In contrast, means and standard errors, though smaller, are about the same size in the eastern Santa Barbara Channel, and the means in some of these locations cannot be distinguished from zero. The standard errors estimated from (1) can be used to estimate the effective number of independent observations per bin; that is,

$$(\delta U_k)^2 = (\sigma_k)^2/N_k \qquad (2)$$

where σ_k is the standard deviation in the k direction and N_k is the number of independent observations in that direction. Comparison of the total number of observations per bin with the independent number of observations (in the major principal axis direction) shows the number of independent observations is much lower, about the same as the number of deployments (Figure 3a). It also shows that though the numbers of observations in the eastern section are higher (due to slower velocities) than in the western section, the numbers of independent observations are similar.

3.2. Comparison to Near-Surface Current Meter Velocities

In Figure 3, drifter mean velocity magnitudes are typically greater than those of VMCMs. We expect some differences to be a function of the instrument used to measure velocity. However, because the comparison in Figure 3 is between continuous VMCM records

Table 1. Observed and Log Layer Surface Velocity Differences

Locations[a]	Number of Observations	$\Delta u_{\log}$[b]	Δu_{obs}	$\Delta v_{\log}$	Δv_{obs}
SMIN:NDBC54	89	2.1	4.4 ± 1.3	-1.0	-1.4 ± 1.4
SMOF:NDBC54	81	3.2	-0.1 ± 1.2	-2.0	-4.7 ± 1.2
ROIN:HONDO	51	0.7	-2.9 ± 1.5	-0.3	-1.3 ± 1.3
ROOF:NDBC54	33	4.4	1.0 ± 2.3	-2.6	0.5 ± 1.8
GOIN:HONDO	44	0.4	-1.1 ± 1.9	0.0	2.3 ± 1.5
GOOF:NDBC53	139	0.2	3.9 ± 1.0	0.2	2.9 ± 0.9
CAIN:NDBC53	150	2.8	3.3 ± 0.7	0.2	1.4 ± 0.7
ANMI:GAIL	92	2.2	4.3 ± 1.2	-0.8	-8.2 ± 1.4

[a]Measurement locations are shown in Figure 4.

[b]Units are in cm s^{-1}. Variables u and v are the east-west and north-south velocity components respectively. The subscript log denotes the log layer shear between 1 and 5 m while the subscript obs denotes the observed shear between 1 m drifters and 5 m current meters.

and discontinuous drifters, it includes sampling differences. To minimize sampling differences and concentrate on instrumental differences, VMCM velocities are here flagged and averaged only when a drifter passes within a 12.5 × 12.5 km^2 bin centered on the VMCM.

Drifter velocity estimates are at a nominal depth of 0.5 m, while VMCM velocities are at a depth of 5 m. The possibility exists for real shear in the upper 5 m. Wind forcing is one source of shear. The near-surface response of the ocean to wind forcing is still uncertain and the subject of active investigation. One model applied to near-surface shear is the logarithmic boundary layer [*Csanady*, 1984; *Richman et al.*, 1987; *Santala*, 1991]. The theoretical estimate of the log layer shear is given by *Richman et al.* [1987]:

$$\Delta \mathbf{u}_{\log} = \mathbf{u}_* \kappa^{-1} \ln(z_1/z_0) \tag{3}$$

where $\mathbf{u}_* = (\tau/\rho_{\mathrm{air}})^{0.5}$ is the shear velocity induced by the wind stress, κ is von Karman's constant (0.4), and $z_1 = 5$ m and $z_0 = 0.5$ m are the depths of the VMCM velocity and drifter velocity estimates respectively. Here $\mathbf{u}_*$ and $\Delta \mathbf{u}_{\log}$ are in the direction of wind velocity.

In Table 1 and Figure 4, the mean velocity shear is compared with that predicted by wind-forced log layer.

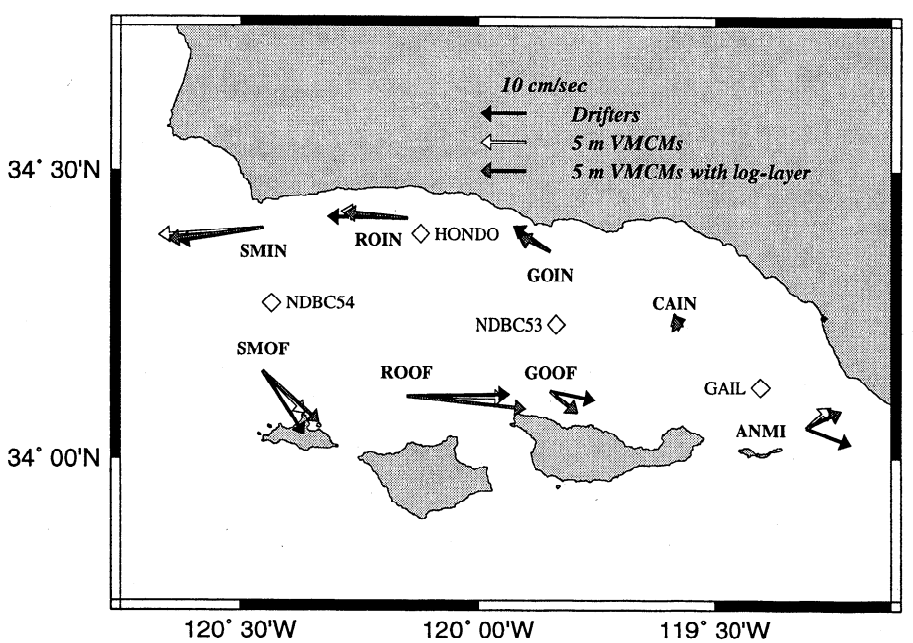

Figure 4. Simultaneous drifter mean velocities (solid arrows), VMCM mean velocities (open arrows), and VMCM mean velocities with a wind-driven logarithmic boundary layer added (shaded arrows).

The strongest winds are found in the southern and western sections of the channel, while weaker and variable winds are usual in the eastern channel and along the north side of the channel east of Point Conception [*Caldwell et al.*, 1986; C. E. Dorman and C. D. Winant, The marine layer in and around the Santa Barbara Channel, submitted to *Monthly Weather Review*, 1998; also by C. E. Dorman as presented by *Winant et al.*, 1996]. Table 1 and Figure 4 show wind-induced shear is generally the same magnitude and sign of the observed shear; however, quantitative agreement is weak and uncertainties in the velocity comparison are generally as large as a predicted log layer shear.

Differences between drifter and current meter velocities also arise owing to wave effects. Drifters are affected by Stokes drift. Current meters also are affected by surface waves. The actual moored VMCM response to waves is complicated and may include VMCM underspeeding [*Richman et al.*, 1987] as well as effects of horizontal mooring motion [*Pollard*, 1973]. However, some estimate of wave-induced velocity differences due to Stokes drift and vertical mooring motions can be made as follows:

$$\mathbf{u}_W = \mathbf{u}_S - \mathbf{u}_M = a^2\sigma k e^{-2kz_0} - 0.5a^2\sigma k e^{-kz_1} \quad (4)$$

where $\mathbf{u}_W$ is the net wave-induced velocity difference, $\mathbf{u}_S$ is the Stokes drift, $\mathbf{u}_M$ is the wave-induced velocity caused by vertical mooring motion [*Pollard*, 1973], a is the wave amplitude, σ is the angular wave frequency, and k is the wave number. For a given wave period, σ and k can be calculated and used in (4) with a.

Estimation of (4) would require an integral average over all wave periods. However, typical wave-induced velocity differences can be gauged from the dominant wave amplitudes, periods, and directions available at National Data Buoy Center (NDBC) buoys 46054 and 46053 (NDBC 54 and 53). At NDBC 54 the median wave amplitude, period and direction of origin between 1994 and 1997 were 1.9 m, 11.1 s, and 295°T respectively. At NDBC 53 they were 1.16 m, 10 s and 269°T between 1994 and 1996. NDBC 54 is representative of locations in the southwest and south Santa Barbara Channel that are affected by open ocean swell from the north Pacific, while NDBC 53 is representative of other locations within the channel that are only directly exposed to waves from the west. The u_W (v_W) caused by waves with these parameters are 3.3 (2.2) and −1.5 (0.0) cm s^{-1} for buoy 54(53).

The wave-induced velocity shears are roughly the same magnitude and direction as those in Table 1, and both may share some responsibility for current meter and drifter velocity differences. Moreover, the separation of wind and wave effects is merely an approximation as they are coupled [e.g., *Gnanadesikan and Weller*, 1995].

Along the relatively sheltered northern channel, wave effects and wind-induced shear have a sign opposite to observed velocity differences. One other possibility is that drifters preferentially sample surface convergences (fronts) with higher velocities. To try to test this, surface drifter temperatures were compared to simultaneous, moored 1-m temperatures. Velocities were sorted by horizontal temperature differences with the reasoning that larger temperature differences might signal the presence of density fronts. However, velocity differences had no clear dependence on horizontal temperature differences.

3.3. Synoptic Variability

Moored velocity observations show the surface circulation exhibits strong variability owing to the occurrence of different synoptic circulation states [*Harms and Winant*, 1998]. These synoptic states (dubbed upwelling, cyclonic, relaxation, and floods) represent the large-scale response of circulation in the Santa Barbara Channel to differing pressure and wind fields.

The upwelling state results from strong equatorward winds in the western channel in combination with weak along-shelf pressure gradients. The winds lead to upwelling near Point Conception. Weak pressure gradients allow cold, upwelled waters to flow south across the channel, continue east along the channel islands, and often exit the channel through the eastern entrance.

The cyclonic state represents a response to strong winds in combination with a strong poleward pressure gradient. It is characterized by flow into the channel through the eastern entrance and a strong cyclonic recirculation in the western channel. The cyclonic recirculation can appear stationary or propagate westward.

Weak winds in combination with a strong poleward pressure gradient lead to a relaxation circulation pattern characterized by strong inflow at the eastern entrance and strong westward flow along the northern coast of the Santa Barbara Channel. Cyclonic recirculation is still present in the western channel, but outflow at the north of the western entrance weakens the southern limb of the recirculation.

If both winds and pressure gradient are weak, the circulation within the channel can be described as a weak, unidirectional, along-channel flow dubbed flood east or flood west.

Cyclonic circulation in the western channel is present under the upwelling, cyclonic, and relaxation patterns, accounting for the strong mean circulation observed in Figure 3. Though the synoptic states do not explain the full response of the circulation, they are useful conceptual models and show up in statistical analyses of the moored observations as described by *Harms and Winant* [1998].

To examine the influence of these synoptic patterns on drifter velocity variability, we employ empirical orthogonal functions (EOFs). Velocities from each deployment are averaged within the same 12.5 km × 12.5 km bins used in Figure 3. EOFs from velocity components are presented since velocities are generally polarized in the along-channel (east-west) direction and the

resulting real modal amplitudes are more readily interpreted. EOFs calculated using complex velocity vectors yield similar results. Consideration of all drifter velocities from a deployment as a single vector assumes they result from a single synoptic state that does not change during the deployment. This is supported by the generally short (relative to the synoptic timescale) times spent by drifters in the channel and by the estimated number of independent observations which is comparable to the number of drifter deployments (Figure 3a).

The first EOF (Figure 5) of drifter velocities consists of east-west velocity fluctuations across most of the Santa Barbara Channel. This mode contains 25% of the variance. When added to the average velocity with an eastward sign, the velocity vectors corresponding to the upwelling synoptic pattern result. When added to the average velocity with a westward sign, velocities correspond to the relaxation pattern. The first EOF mode of drifter velocities is very similar to the first mode of surface current meter velocities discussed by *Harms and Winant* [1998]. Their first mode also corresponds to upwelling and relaxation synoptic patterns and accounts for a similar percentage of the variance. The close correspondence between the first drifter and current meter modes is gratifying in that the types of velocity data are in some ways quite different. The drifter data contain velocity information throughout the Santa Barbara Channel including locations where no current meters were present. The current meter data contain continuous information regarding temporal variability as well as data from current meters north of Point Conception and in the eastern Santa Barbara Channel beyond the easternmost drifter deployment location.

The second EOF (Figure 5) of drifter velocities consists of cyclonic (or anticyclonic if the sign is reversed) fluctuations in the western part of the channel with east-west velocity fluctuations across the northern, mainland coast of the Santa Barbara Channel. This mode contains 14% of the variance. When added to the average with a cyclonic sign, the result corresponds to a strengthening of cyclonic circulation, and when added with an anticyclonic sign, it corresponds to a weakening of the cyclonic circulation. Like the first drifter EOF mode, the second drifter EOF mode corresponds with an EOF mode in the current meter velocities in structure and variance.

Neither the separation of the first two EOFs into two distinct modes nor the identification of these modes with two different synoptic states is perfect. Given the number of deployments (23) and the modal eigenvalues, confidence levels [*North et al.*, 1982] for the first two modal eigenvalues overlap (barely) at the 95% level, indicating they may not be entirely distinct. The first two modes account for 39% of the variance. Higher modes include more of the variance (four modes account for 58% of the variance and six modes account for 73%); however, confidence levels for these modes overlap to an even greater degree, and they are not easily associated with physical processes as the first two modes are.

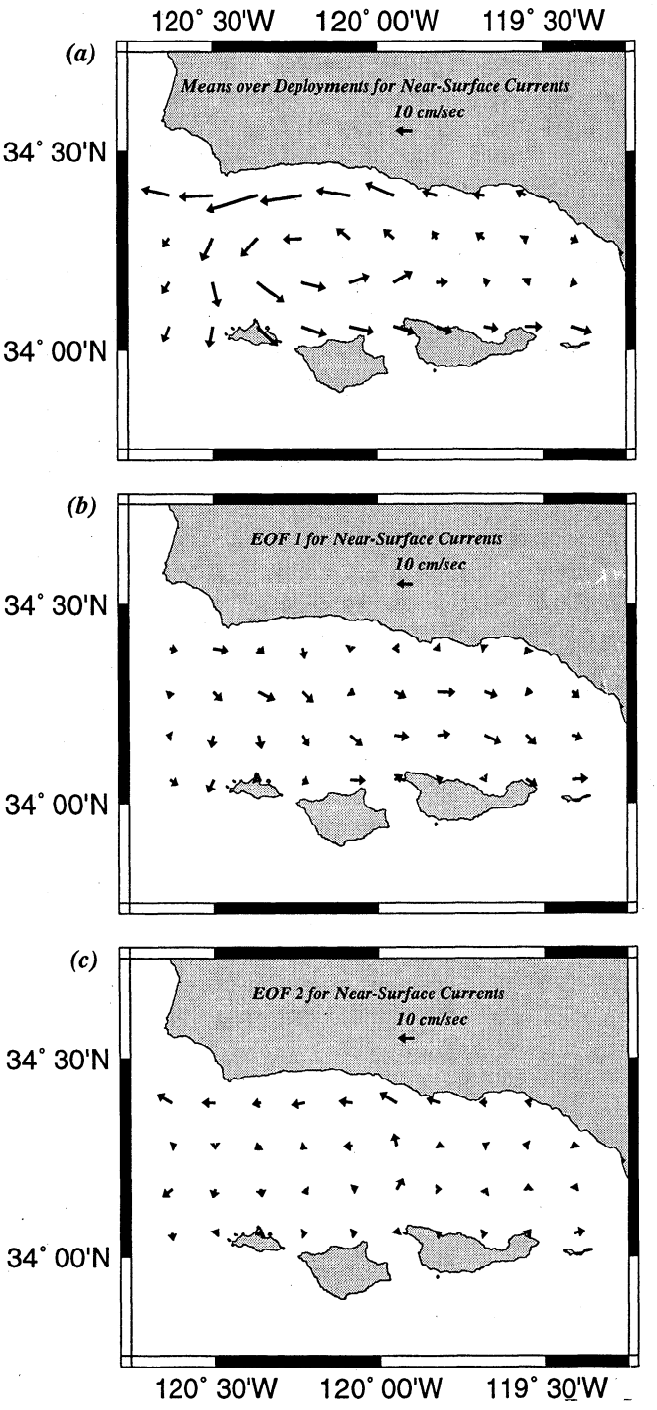

Figure 5. (a) Average over individual drifter deployments. (b) The first empirical orthogonal function (EOF) which, added to the average, is consistent with the upwelling pattern. The first EOF subtracted from the average resembles the relaxation pattern. (c) The second EOF which. added to the average, enhances the cyclonic circulation in the western Santa Barbara Channel. The second EOF subtracted from the average weakens the cyclonic circulation.

Modal amplitudes of the first two EOFs (Figure 6) show that the first EOF usually occurs in spring with a

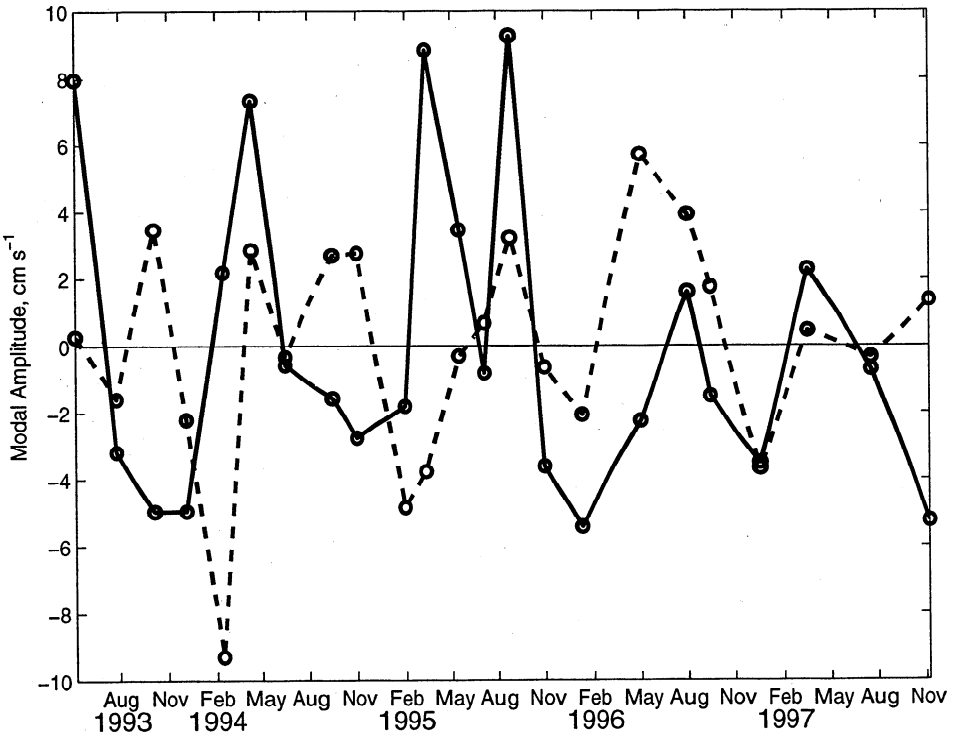

Figure 6. Modal amplitudes for first two drifter EOFs. Amplitudes for the first EOF (circles, solid lines) are generally positive in spring, indicating eastward flow (especially along the southern Santa Barbara Channel) and negative in fall, indicating westward flow relative to the mean. Amplitudes for the second EOF (circles, dashed lines) are generally positive in summer and fall, indicating strengthened cyclonic flow relative to the mean, and negative in winter, indicating weakened cyclonic flow relative to the mean.

sign consistent with the upwelling pattern and in the fall with a sign consistent with the relaxation pattern. Exceptions to this occur in August 1995, when a late summer upwelling event took place, and in May 1996, when the cyclonic mode dominates. The second EOF mode generally enhances the cyclonic flow in summer while subtracting from it (and leading to an overall weaker flow) in winter.

3.4. Seasonal Averages

Seasonal variation in the prevalence of the synoptic states (Figure 6) affects the seasonal averages. It is important to note that only five to seven deployments exist for each season; hence the statistical reliability for seasonal drifter velocity averages is low. Nonetheless, the correspondence to synoptic variability and the comparison to moored observations is encouraging.

In spring (March, April, and May) the upwelling and cyclonic patterns dominate. Both the drifters and VMCMs (Figure 7) show southward flow at the western channel entrance and eastward flow along the southern boundary of the channel which, at the resolution of the map, continues out past the eastern entrance. The eastward flow along the southern edge is stronger than that over all drifter deployments (Figure 3). Despite the low number of independent observations, it is greater than the standard error. The predominance of the upwelling state means flow at the western entrance is not well described by the available spring observations where little data exist and standard errors are largest. The fluctuating kinetic energy (Figure 7d) is measured relative to the spring average. It is highest in the western channel and at the eastern entrance. However, the maximum at the western entrance is defined by only a few independent observations.

The upwelling, cyclonic, and relaxation states can all occur in summer (June, July, and August). There is generally good agreement between the VMCMs and drifters (Figure 8), except near the eastern entrance to the channel where drifters preferentially sample the upwelling state. Summer average velocities are quite strong and are often larger than principal axis standard deviations, particularly in the western half of the channel. The summer averages also show a well-developed cyclonic circulation. Relative to spring, flow in the eastern channel is weakened, while westward flow along the northern boundary is strengthened. The fluctuating kinetic energy shows a maximum in the western entrance extending to the western tip of Santa Cruz Island. It resembles that in Figure 3.

The cyclonic and relaxation states prevail in fall (September, October, and November) (Figure 9). The up-

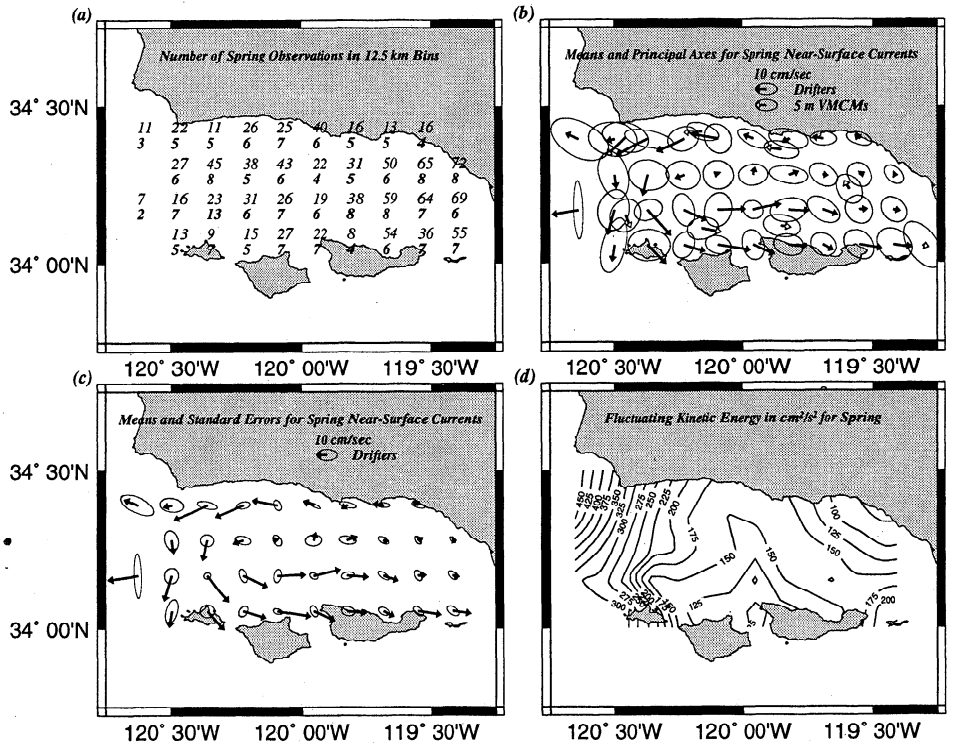

Figure 7. Same as Figure 3, but for spring (March, April, and May) deployments. Fluctuating kinetic energies are defined relative to the spring average.

welling state seldom occurs as indicated by the low number of drifter observations in the extreme eastern channel. The fall averages are distinguished by the strengthening of westward flow along the northern edge of the channel with weakening of the southern limb of the cyclonic circulation. Many drifters exit the western entrance, turning past Point Conception and heading north along the central California coast. Reasonably good agreement exists between VMCMs and drifters during this time. The fall fluctuating kinetic energy re-

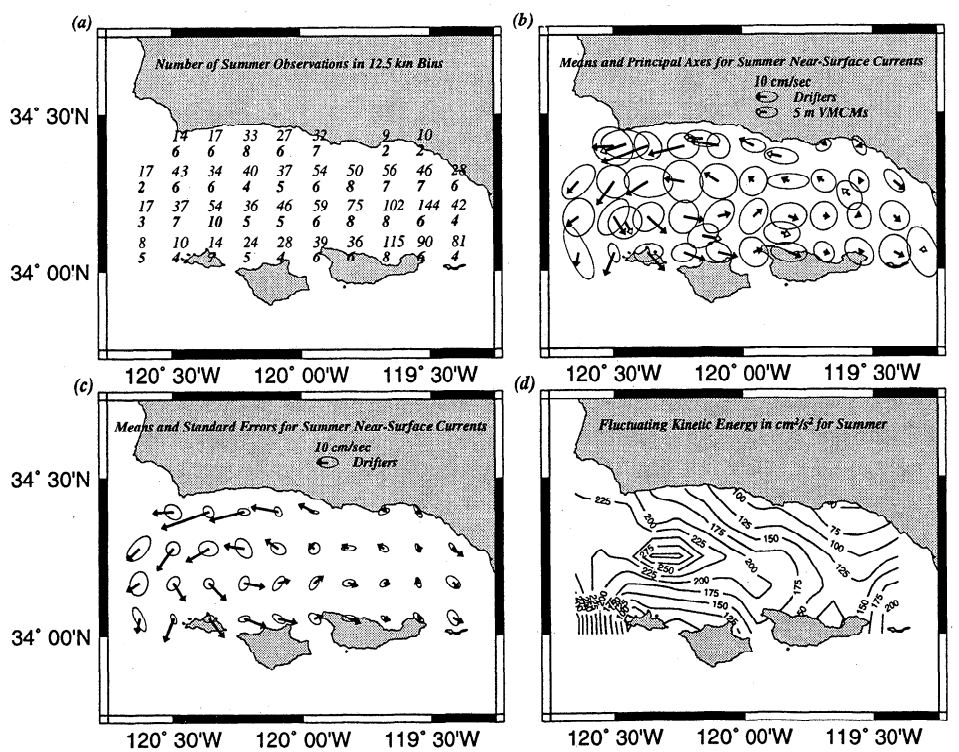

Figure 8. Same as Figure 3, but for summer (June, July, and August) deployments. Fluctuating kinetic energies are defined relative to the summer average.

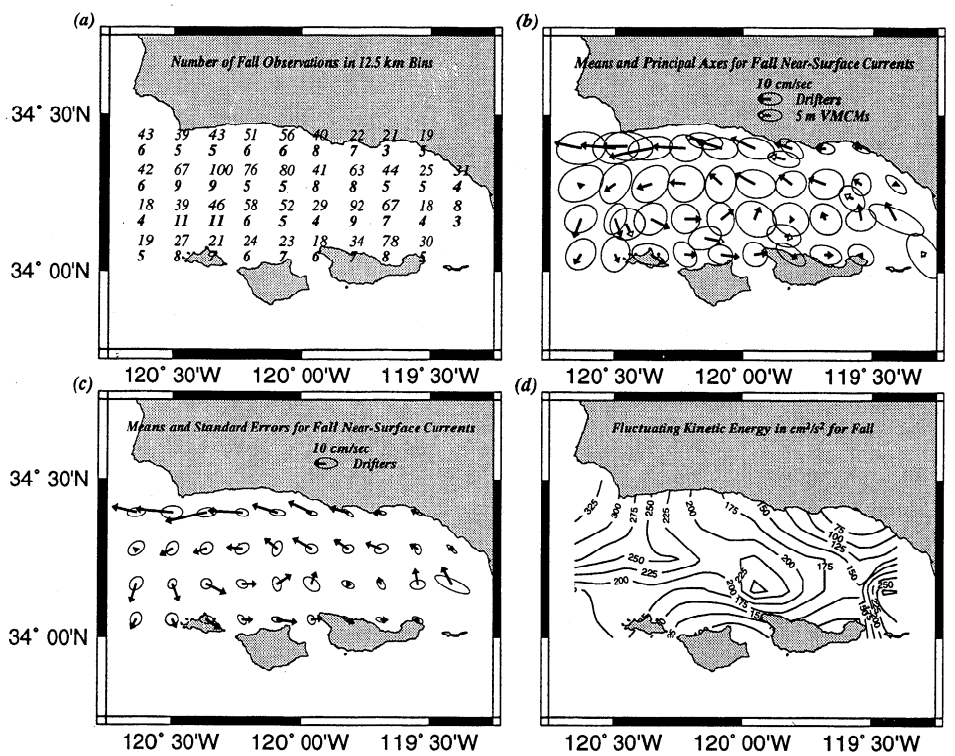

Figure 9. Same as Figure 3, but for fall (September, October, and November) deployments. Fluctuating kinetic energies are defined relative to the fall average.

sembles that for Figure 3, except north of Santa Cruz Island where contours enclose a secondary maximum and at the eastern entrance where few observations exist.

Mean winds and pressure gradients tend to weaken in winter (December, January, and February), and the winter circulation has weak average velocities and low standard deviations relative to other seasons (Figure 10). This is also evident in the low fluctuating kinetic energies which have relatively little spatial structure. The

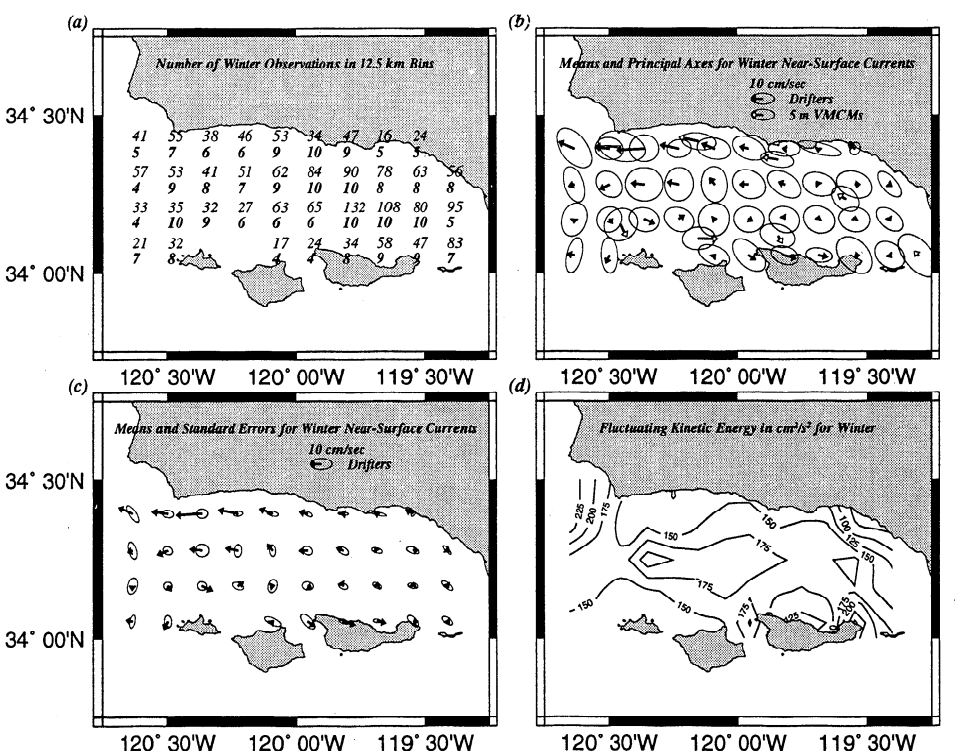

Figure 10. Same as Figure 3, but for winter (December, January, and February) deployments. Fluctuating kinetic energies are defined relative to the winter average.

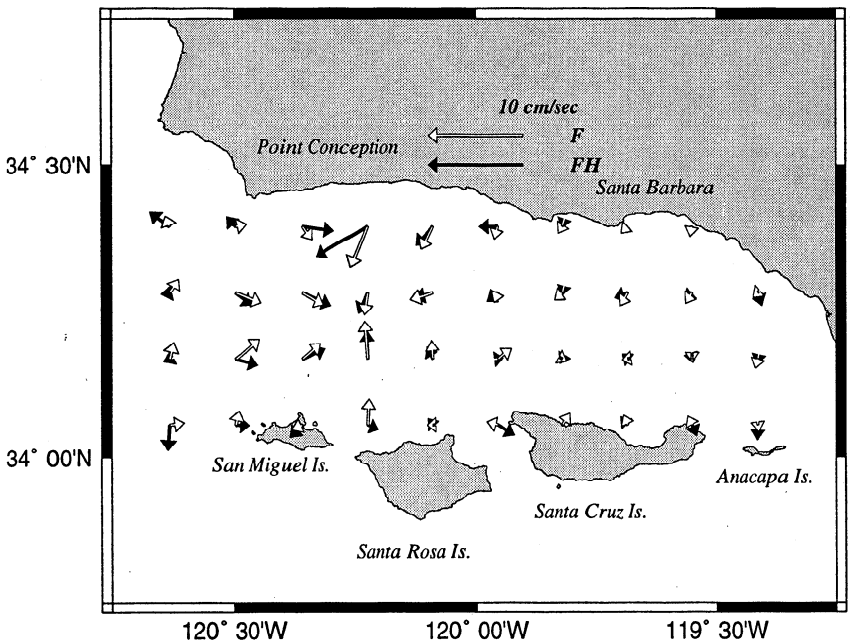

Figure 11. Horizontal eddy stress divergence $\mathbf{F_H}$ (solid arrows) and total eddy stress divergence $\mathbf{F}$ (open arrows) as estimated by the mean Lagrangian acceleration. $\mathbf{F}$ and $\mathbf{F_H}$ are scaled by $1/\rho f$, where ρ is density and f is the Coriolis parameter to give velocity units.

spatial distribution of winter drifter velocities is reminiscent of the relaxation pattern. Principal axes standard deviations exceed averages, except for the westward flow in the northwest channel. Comparison with the VMCMs is generally good; however, winter mean velocities throughout most of the channel are smaller than their standard errors.

4. Mean Surface Momentum Balance

The mean surface momentum balance is estimated after *Davis* [1985b] as

$$\rho \mathbf{f} \times \langle \mathbf{u} \rangle + \nabla P - \partial_z \tau = -\rho \nabla \cdot \langle \mathbf{uu} \rangle - \rho \partial_z \langle w\mathbf{u} \rangle \quad (5)$$

where ρ is the density, $\mathbf{f}$ is the Coriolis parameter, $\mathbf{u}$ is the horizontal velocity, P is the pressure, τ is the wind stress, $\rho\nabla\cdot\langle\mathbf{uu}\rangle$ is the eddy stress divergence due to horizontal advection, and $\rho\nabla \cdot \langle \mathbf{uu} \rangle + \rho\partial_z\langle w\mathbf{u} \rangle$ is the total eddy stress divergence. Drifter data allow direct estimation of the horizontal eddy stress divergence $\mathbf{F_H}$ from spatial gradients of velocity products. The total eddy stress divergence $\mathbf{F}$ can be estimated from the mean Lagrangian acceleration [*Davis*, 1985b] with the assumption that vertical scales of $\mathbf{u}$ fluctuations are greater than the depth at which drifters follow the flow.

The eddy stress divergence terms $\mathbf{F_H}$ and $\mathbf{F}$ (Figure 11) are scaled by $1/(\rho f)$ so that they are in velocity units. The horizontal Reynolds stress divergence estimates are generally similar in magnitude and direction (within about 45°) to the total Reynolds stress divergence estimates derived from mean Lagrangian accelerations. The magnitudes of the estimates range from 0.01 to 0.05 m s^{-1}. The largest values of $\mathbf{F}$ and $\mathbf{F_H}$ tend to be in the western Santa Barbara Channel (SBC) in the region of mean cyclonic flow.

In comparison to the CODE area [*Davis*, 1985b], the magnitudes of Reynolds stress divergence are similar. The maximum magnitudes in the SBC may be slightly larger than in the CODE region, which has maxima around 0.03 m s^{-1}. There is also a closer correspondence between $\mathbf{F_H}$ and $\mathbf{F}$ in the Santa Barbara Channel, especially in the western cyclone. This indicates a greater importance of horizontal advection and reduced upwelling in the SBC relative to CODE. In making this comparison, we emphasize that *Davis* [1985b] looked at a coastal upwelling region during the season of maximum upwelling, while the SBC drifter data are taken over all seasons and several years.

The total Reynolds stress divergence $\mathbf{F}$ is much smaller than the mean surface velocity (Figure 12). In general, the mean velocities are at least a factor of 5 larger, particularly along the northern and southern boundaries of the SBC. The Reynolds stress divergence is strongest in the western SBC. There it is consistently 90° to the left of the mean surface velocity. By (5), the mean flow driven by $\mathbf{F}$ is 90° to its left, so it acts to slow the mean flow, particularly in the western SBC.

Other terms in (5) include the wind stress and pressure gradient. The mean wind stress τ is plotted at measurement locations (Figure 12). The surface velocity due to the mean wind stress depends on the vertical mixing of momentum within the surface boundary layer. For a well-mixed surface boundary layer with a depth of 10 m the surface velocity magnitude would equal the

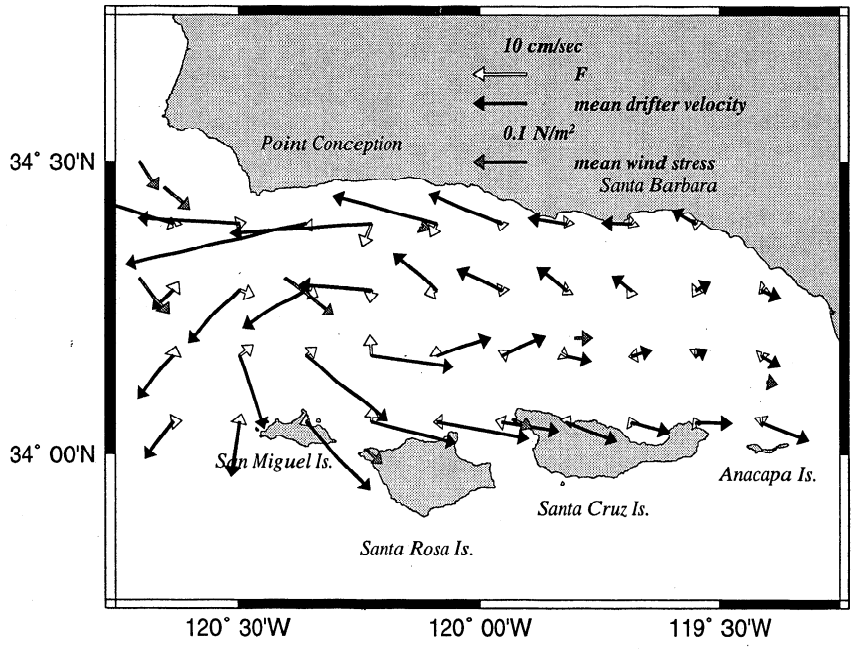

Figure 12. Mean Lagrangian acceleration **F** (open arrows). near-surface velocity (solid arrows), and wind stress (shaded arrows). Wind stress (shown at measurement locations) is also shown. Velocity forced by **F** is 90° to the left of arrows. Note change in scale from Figure 11.

wind stress arrow length with a direction 90° to the right of the wind stress vectors shown. These magnitudes are less than the observed mean velocity everywhere but are comparable in the western channel. If momentum in the surface boundary layer were not well mixed (as in the logarithmic boundary layer explored in section 3.2), wind-forced drifter velocities could be more nearly parallel to the wind.

The cyclonic circulation in the western Santa Barbara Channel strongly suggests the presence of a mean low pressure centered there. No direct estimates of the pressure gradient exist with sufficient spatial and temporal resolution to resolve the mean pressure gradient. However, synoptic survey XBT and CTD sections (according to E. D. Lawson as presented by *Winant et al.* [1996]) in the western basin often show baroclinic pressure gradients with geostrophic velocities similar to those observed with the drifters and current meters.

5. Lagrangian Statistics

5.1. Single Particle Diffusivity

In this section, we estimate the single particle diffusivity κ for the eastern and western halves of the Santa Barbara Channel. As *Swenson and Niiler* [1996] point out, κ is nonlocal and depends on the time history of the flow. For an inhomogeneous flow, there are limits on the area over which κ can be sensibly calculated. Figure 3 shows that the flow field varies strongly in its means and variabilities within the Santa Barbara Channel. The challenge is to identify an area large enough such that a particle is likely to remain within the area for the duration of the single particle diffusivity calculation, but small enough to be descriptive of some aspect of the flow. We calculate κ over two 50 km by 50 km bins covering the eastern and western halves of the Santa Barbara Channel. The western bin is defined by the second through fifth columns of bins shown in Figure 3. It extends from the western tip of San Miguel to the western tip of Santa Cruz and covers the region with generally higher mean velocities and fluctuating kinetic energies, as well as the large western cyclonic cell. The eastern bin is defined by the sixth through ninth columns of bins shown in Figure 3. It extends from the western to the eastern tips of Santa Cruz and covers the region in which generally low mean velocities and fluctuating kinetic energies are observed. The bins exclude the areas most likely affected by array bias and are large enough so the mean distance over which particles travel during the single particle diffusivity calculation (5 days) is approximately 35 km in the western half of the basin and 25 km in the eastern half of the basin.

The single particle diffusivity can, under certain conditions [*Davis*, 1987, 1991], be used quantitatively to model diffusion. These conditions include (1) a scale separation in which the average predictable displacement for a particle is smaller than its unpredictable displacement for times greater than the Lagrangian decorrelation timescale and (2) the average unpredictable displacement for a particle is smaller than the spatial scales over which it varies. These conditions are not met on the scales for which we can estimate κ in the Santa Barbara Channel. The unpredictable or diffusive part

of the flow varies on the same scales as the mean flow (i.e., from the western to eastern halves of the channel). Therefore κ is here presented simply as a statistic that can highlight certain features of the flow.

The single particle diffusivity is calculated after *Davis* [1991].

$$\kappa_{jk}(\mathbf{x},t) = -\langle v_j'(t_0|\mathbf{x},t_0)d_k'(-t|\mathbf{x},t_0)\rangle \qquad (6)$$

where j and k are indices representing components of the flow and v' and d' are fluctuating Lagrangian velocities and displacements. We integrate v' and d' over quarter-day intervals for up to 5 days. The methods used to determine average Lagrangian velocities and displacements and their fluctuations follow those of *Swenson and Niiler* [1996].

The single particle diffusivities (Figure 13) are shown for east-west (κ_{xx}), north-south (κ_{yy}), and asymmetric (κ_A) elements. The asymmetric part of κ is defined by $\kappa_A(t) = \kappa_{xy} - \kappa_{yx}$. Figures 13a and 13b show that κ generally increases for times less than 2 days, after which it levels or drops. Here κ_{xx} is greater than κ_{yy} in both the eastern and western halves of the Santa Barbara Channel. This is due to greater autocovariance in the east-west (along channel) direction and to the longer timescales of fluctuations in this direction. Both κ_{xx} and κ_{yy} are greater in the western basin owing to the stronger fluctuations observed there. Another feature that is readily apparent in Figure 13 is the difference in κ_A between the western and eastern halves of the basin. The magnitude of κ_A in the western half of the basin, where the cyclonic cell is dominant, is much larger than in the eastern half. This is also manifested in the time dependence of κ_{xx} and κ_{yy} in the western half of the basin. Lagrangian velocity and displacement components for drifters occupying the western cyclonic cell become negatively correlated as they are carried to the opposite side of the cell. This causes the decline in single-particle diffusivities for times longer than 1.5–2 days.

5.2. Lagrangian Time and Space Scales

Lagrangian time and space scales can be estimated from the single particle diffusivity for large time κ^∞ as $T = \kappa^\infty/\langle v'^2\rangle$ and $L = \kappa^\infty\langle v'^2\rangle^{-1/2}$ [*Davis*, 1991; *Rossby et al.*, 1983; *Krauss and Böning*, 1987]. If the maxima of κ_{xx} and κ_{yy} are taken as κ^∞, then T_x = 0.4 (0.5) days, T_y = 0.3 (0.2) days, L_x = 9 (8) km and L_y = 5 (3) km for the western (eastern) basins. Figure 13 suggests this method has limitations in the western half of the Santa Barbara Channel in that κ_{xx} and κ_{yy} do not reach steady state values and decline after 1.5 days. The behaviors of κ_{xx} and κ_{yy} and κ_A suggest fluctuations in the cyclonic or anticyclonic sense are correlated for longer than 1 day. In contrast, a plausible interpretation of T_x, T_y, L_x and L_y in the eastern SBC is that a typical particle's "memory" of its past velocity fluctuations is less than 1 day and only extends over the region it has traveled in that time.

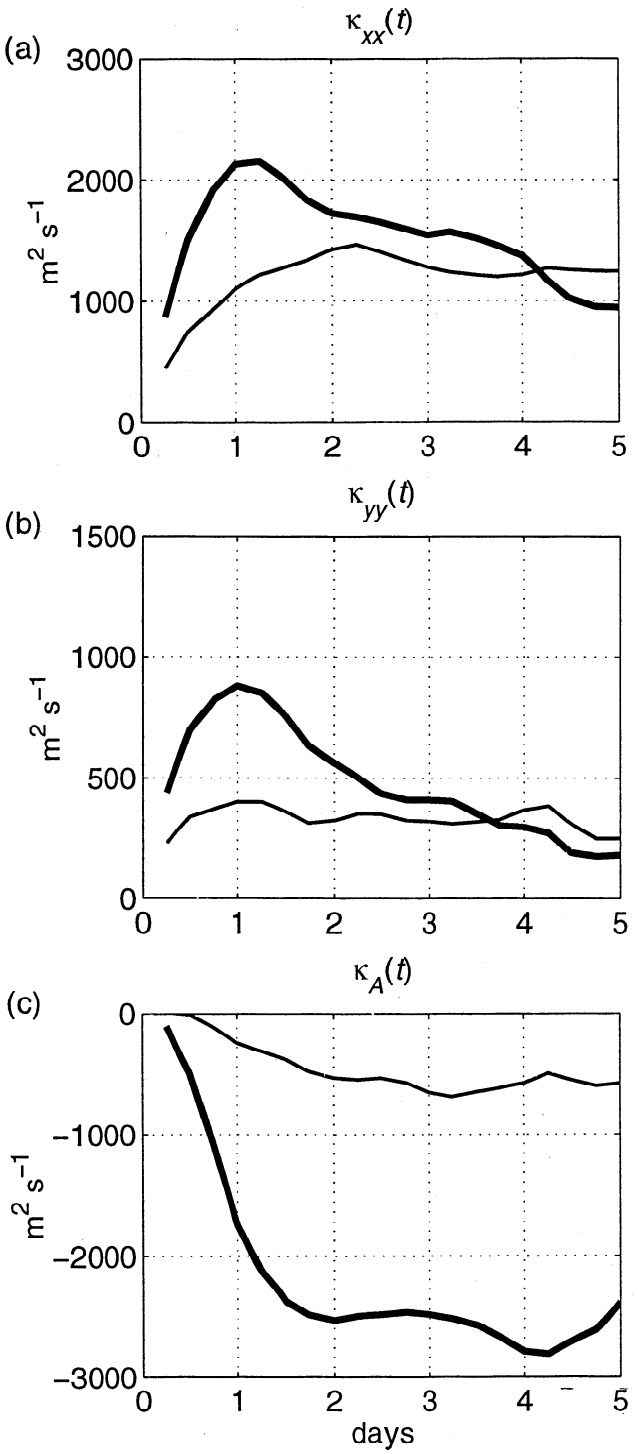

Figure 13. Single-particle diffusivities in the eastern (thin line) and western (thick line) Santa Barbara Channel for the (a) east-west, (b) north-south, and (c) asymmetric elements. Note that the vertical scale on Figure 13b is reduced by a factor of 2 relative to Figures 13a and 13c. Cyclonic circulation in the western Santa Barbara Channel (indicated by the large negative κ_A in Figure 13c) is responsible for the decline in κ_{xx} and κ_{yy} there.

Autocorrelations provide another estimate of the Lagrangian timescales. We calculate along-channel (r_{uu}), cross-channel (r_{vv}), and complex [following *Kundu*, 1976] autocorrelations (r_c) averaged over drifters for the same

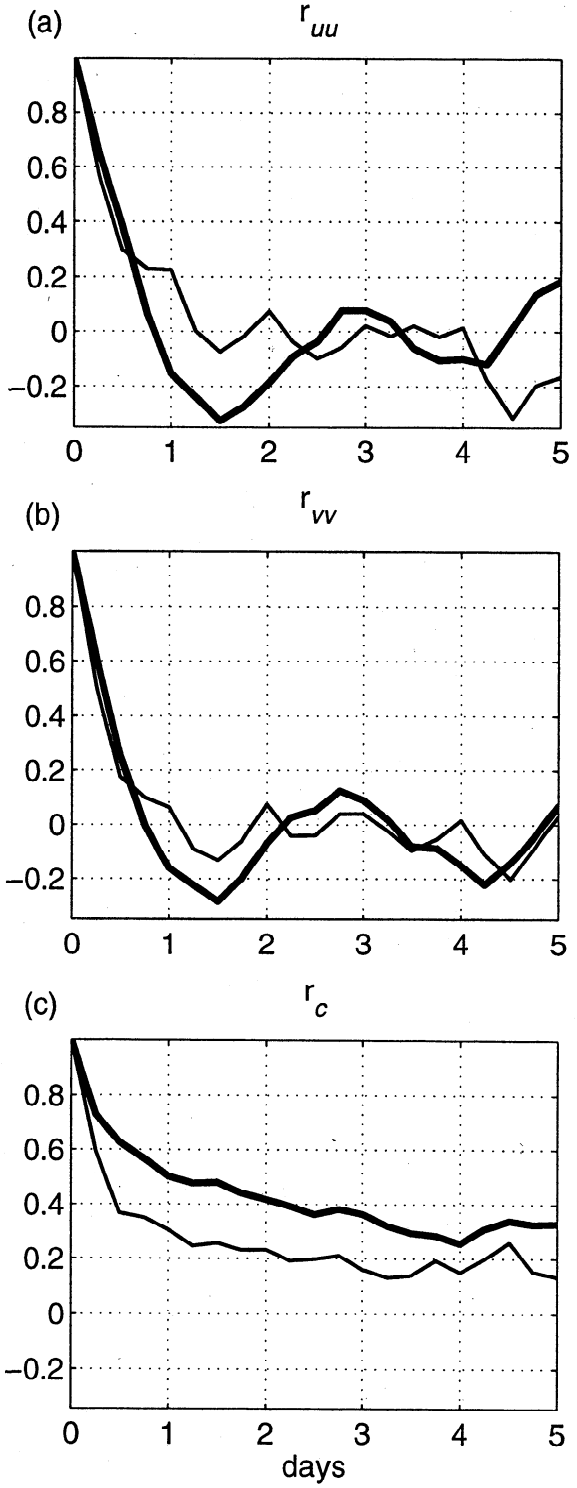

Figure 14. Averaged Lagrangian autocorrelations in the eastern (thin line) and western (thick line) Santa Barbara Channel for the (a) east-west (u), (b) north-south (v) velocity components, and (c) the complex autocorrelation coefficient.

regions as κ. We consider only segments of Lagrangian velocity time series located entirely within one half of the channel or the other and lasting 6 days or longer. Correlations are calculated out to a maximum lag of one half the time series length.

The autocorrelations (Figure 14) show a number of interesting features. In the western half of the basin, u and v are negatively correlated at lags of 2–4 days. As with κ, this indicates drifters moving from one side of the cyclonic circulation to the other. The complex autocorrelation takes account of this and shows modest correlation to a lag of 4 days. Autocorrelations in the eastern Santa Barbara Channel show less tendency for cyclonic motion. Both r_{uu} and r_{vv} decline to near zero within 1.5 days and remain near zero without a negative correlation becoming apparent. The complex correlation in the eastern Santa Barbara Channel also declines to 0.2 within 1.5 days. Autocorrelations in the eastern and western basin also show inertial and tidal oscillations do not dominate the Lagrangian velocity fluctuations, as little evidence of peaks near 12 or 24 hours exists.

Lagrangian timescales estimated from κ or the autocorrelation (Figure 14) are less than Eulerian timescales (Figure 2). Lagrangian timescales are affected by the total acceleration including advection while the Eulerian timescales are a function only of the local acceleration; hence they are an indicator of the importance of nonlinearity to the evolution of the time-varying velocity field [*Davis*, 1985b]. The difference in Eulerian and Lagrangian timescales strongly suggests advection is important in the fluctuating velocity field. This is also true in the CODE region off northern California.

6. Conclusions

Argos-tracked surface drifters were deployed between May 1993 and November 1997 in the Santa Barbara Channel, with the general goals of aiding the description of the general circulation and providing direct estimates of surface parcel trajectories. The specific objectives of this study were to assess the drifter sampling statistically; to use the drifter data to aid in the description of the synoptic, seasonal, and mean circulation; and to estimate Lagrangian scales of motion.

The estimates of the mean surface circulation generally agree with near-surface current meter measurements and add detail beyond that provided by the current meters. The dominant feature of the mean circulation is the presence of cyclonic circulation in the western half of the channel. The mean flow here is about 0.15–0.20 m s^{-1} and is larger than the variance about the mean. The mean drifter velocities also show a bifurcation at the eastern side of the cyclonic circulation north of Santa Cruz Island. Flow can either turn north and west into the cyclonic circulation or continue east along the north side of Santa Cruz Island. Drifters also make clear the relatively weak flow in the northeast channel over the broad shelf between Santa Barbara and Port Hueneme. Standard deviations along principal axes are aligned with mainland and island coasts at the northern and southern edges of the channel. Relatively little polarization is observed in the central channel.

Mean velocity estimates derived from the drifters and current meters agree generally in magnitude and direction. Drifter velocity estimates are generally higher than current meter estimates. The exception to the general agreement occurs at the eastern entrance to the channel. This region is outside the drifter deployment area, and comparison to the moored measurements indicates drifter velocity estimates are biased toward outflow (eastward velocity) conditions. Nearby drifter and current meter velocities are also compared at simultaneous times. This comparison indicates that even for simultaneous velocities, drifter velocity magnitudes tend to be somewhat higher. As the current meters sample at 5 m and the drifters sample above 1 m, this near-surface current shear may, in part, be real. The direction and magnitude of velocity differences are generally in line with wind (logarithmic boundary layer) and wave (Stokes drift) effects, but quantitative agreement is weak.

Drifter observations are also used to examine variability at synoptic and seasonal timescales. Empirical orthogonal functions (EOFs) of drifter data identify spatial patterns of variability which correspond to synoptic patterns of circulation. Upwelling off Point Conception with eastward flow through most of the Santa Barbara Channel is most often observed in spring and summer, strong cyclonic circulation is seen in summer and fall, poleward flow (relaxation) occurs in fall and winter, and along-channel flow (floods) takes place in winter. Mode 1 represents upwelling and relaxation, while mode 2 represents a strengthening or weakening of the cyclonic circulation. These synoptic patterns were also identified in moored observations. Seasonal averages of drifter observations are consistent with seasonal changes in the occurrence of different synoptic patterns.

The drifter velocities provide estimates of the horizontal and total eddy stress divergence in the mean surface momentum balance. Within the western cyclonic circulation the horizontal and total eddy stress divergences agree closely. This indicates horizontal rather than vertical eddy stress divergence dominates. This is in contrast to the Coastal Ocean Dynamics Experiment (CODE) region between Point Arena and Point Reyes where horizontal and total eddy stresses appear quite different. The eddy stress divergence is largest in the western Santa Barbara Channel where its direction consistently opposes Coriolis acceleration of the mean flow. However, it is much smaller than this term, leaving the mean pressure gradient and surface Ekman flow responsible for balancing the Coriolis force. This suggests models emphasizing linear dynamics should provide insight into the mean circulation. This does not mean that nonlinear dynamics are unimportant. The fluctuating flow is almost certainly highly nonlinear as indicated by the differing Lagrangian and Eulerian autocorrelation scales (2–4 and 5–7 days, respectively).

Single-particle diffusivities reflect a strong tendency for cyclonic motion in the western Santa Barbara Channel. The along-channel single-particle diffusivity is substantially greater than the cross-channel single-particle diffusivity. The single-particle diffusivity does not represent small-scale eddy diffusion in the western Santa Barbara Channel, where it is dominated by a large scale cyclonic cell. Single-particle diffusivity as a measure of small-scale eddy diffusion is perhaps more applicable to the eastern channel, which does not contain strong large-scale features.

The drifter deployment pattern and times were chosen to sample the mean circulation and its variability within the Santa Barbara Channel. Estimates of statistical uncertainty and comparisons with moored time series indicate these goals were largely met. One natural question that arises is how successful would a similar drifter program be in other coastal regions? The confines of the Santa Barbara Channel may, in part, lead to success in obtaining relatively unbiased estimates. On a more open coast, upwelling or some other intermittent process may sweep drifters rapidly away from the coast. It is therefore possible that drifter velocities on a more open coast are biased toward conditions in which they tend to remain near the coast (e.g., downwelling). This is one question we plan to examine with a similar study underway in the Santa Maria Basin region immediately north of Point Conception.

Acknowledgments. Support for this work was provided by Cooperative Agreement 14-35-0001-30571 between the Minerals Management Service and the University of California, San Diego. Postdoctoral support for E. P. Dever was provided by a grant from the Mellon Foundation. A great number of people are to thank for the success of the drifter program. First and foremost among these is Douglas Alden (Scripps Institution of Oceanography), who engineered and constructed the drifters. We also thank Shane Anderson and Chris Gotschalk (University of California, Santa Barbara), who carried out numerous drifter deployments from small boats. Thanks also to Sabine Harms (SIO) for discussions regarding the moored data and EOFs and to Nan Bray (SIO) for discussions regarding the comparison of the moored and drifter velocities.

References

Atkinson, L. P., K. H. Brink, R. E. Davis, B. H. Jones, T. Paluskiewicz and D. W. Stuart, Mesoscale hydrographic variability in the vicinity of Points Conception and Arguello during April–May 1983: The OPUS 1983 Experiment, *J. Geophys. Res., 91,* 12,899–12,918, 1986.

Auad, G., Circulation in the Santa Barbara Channel: Description, mass and heat budgets and forcing during 1984, Ph.D. thesis, Scripps Inst. of Oceanogr., Univ. of Calif., San Diego, La Jolla, Calif., 1996.

Auad, G., M. C. Hendershott, and C. D. Winant, Wind-induced currents and bottom-trapped waves in the Santa Barbara Channel, *J. Phys. Oceanogr., 28,* 85–102, 1998.

Barth, J. A., and K. H. Brink, Shipboard acoustic Doppler profiler velocity observations near Point Conception: Spring 1983, *J. Geophys. Res., 92,* 3925–3943, 1987.

Brink, K. H. and R. D. Muench, Circulation in the Point Conception-Santa Barbara Channel region, *J. Geophys. Res., 91,* 877–895, 1986.

Brink, K. H., D. W. Stuart, and J. C. Van Leer, Observations of the coastal upwelling region near 34°30′N off California: Spring 1981, *J. Phys. Oceanogr., 14,* 378–391, 1984.

Caldwell, P. C., D. W. Stuart, and K. H. Brink, Mesoscale wind variability near Pt. Conception, California during Spring 1983, *J. Clim. Appl. Meteorol., 25,* 1241–1254, 1986.

Csanady, G. T., The free surface turbulent shear layer, *J. Phys. Oceanogr., 14,* 402–411, 1984.

Davis, R. E., Drifter observations of coastal surface currents during CODE: The method and descriptive view, *J. Geophys. Res., 90,* 4741–4755, 1985a.

Davis, R. E., Drifter observations of coastal surface currents during CODE: The statistical and dynamical views, *J. Geophys. Res., 90,* 4756–4772, 1985b.

Davis, R. E., Modeling eddy transport of passive tracers, *J. Mar. Res., 45,* 635–666, 1987.

Davis, R. E., Observing the general circulation with floats, *Deep Sea Res., Part I, 38,* S531–S571, 1991.

Gnanadesikan, A., and R. A. Weller, Structure and instability of the Ekman spiral in the presence of surface gravity waves, *J. Phys. Oceanogr., 25,* 3148–3171, 1995.

Gunn, J. T., P. Hamilton, H. J. Herring, L. H. Kantha, and G. S. E. Lagerloef, Santa Barbara Channel Circulation Model and field study, vols. 1 and 2, *Tech. Rep. MMS 87-0089,* 393 pp., Dynalysis, Princeton, N.J., 1987.

Harms, S., Circulation induced by winds and pressure gradients in the Santa Barbara Channel, Ph.D. thesis, Scripps Inst. of Oceanogr., Univ. of Calif., San Diego, La Jolla, Calif., 1996.

Harms, S., and C. D. Winant, Characteristic patterns of the circulation in the Santa Barbara Channel, *J. Geophys. Res., 103,* 3041–3065, 1998.

Hendershott, M. C., and C. D. Winant, Surface circulation in the Santa Barbara Channel, *Oceanography, 9,* 114–121, 1996.

Kolpack, R. J., *Biological and Oceanographical Survey of the Santa Barbara Channel Oil Spill 1969-1970,* vol. 2, 477 pp., Allen Hancock Found., Univ. of South. California, Los Angeles, 1971.

Krauss, W., and C. W. Böning, Lagrangian properties of eddy fields in the northern Atlantic as deduced from satellite-tracked buoys, *J. Mar. Res., 45,* 259–291, 1987.

Kundu, P. K., Ekman veering observed near the ocean bottom, *J. Phys. Oceanogr., 6,* 238–242, 1976.

North, G. R., T. L. Bell, R. F. Cahalan, and and F. J. Moeng, Sampling errors in the estimation of empirical orthogonal functions, *Mon. Weather Rev., 110,* 699–706, 1982.

Pollard, R., Interpretation of near-surface current meter observations, *Deep Sea Res., 20,* 261–268, 1973.

Poulain, P.-M., A. Warn-Varnas, and P. P. Niiler, Near-surface circulation of the Nordic seas as measured by Lagrangian drifters, *J. Geophys. Res., 101,* 18,237–18,258, 1996.

Richman, J. G., R. A. de Szoeke, and R. E. Davis, Measurements of near-surface shear in the ocean, *J. Geophys. Res., 92,* 2851–2858, 1987.

Rossby, H. T., S. C. Riser, and A. G. Mariano, The western North Atlantic — A Lagrangian viewpoint, in *Eddies in Marine Science,* edited by A. R. Robinson, pp. 66–91, Springer-Verlag, New York, 1983.

Santala, M. J., Surface-referenced current meter measurements, Ph.D. thesis, Mass. Inst. of Technol./Woods Hole Oceanogr. Inst., Woods Hole, Mass., 1991.

Smith, R. L., A comparison of the structure and variability of the flow field in three coastal upwelling regions: Oregon, northwest Africa and Peru, in *Coastal Upwelling, Coastal Estuarine Stud.*, vol. 1, edited by F. A. Richards, pp. 107–118, AGU, Washington, D.C., 1981.

Swenson, M. S., and P. P. Niiler, Statistical analysis of the surface circulation of the California Current, *J. Geophys. Res., 101,* 22,631–22,645, 1996.

Winant, C. D., R. C. Beardsley, and R. E. Davis, Moored wind, temperature, and current observations made during coastal ocean dynamics experiments 1 and 2 over the northern California shelf and upper slope, *J. Geophys. Res., 92,* 1569–1604, 1987.

Winant, C. D., et al.; Analysis and acquisition of observations of the circulation on the California Continental Shelf: Quality review board minutes, *Meet. 5,* 653 pp., Cent. for Coastal Stud., Scripps Inst. of Oceanogr., Univ. of Calif., San Diego, La Jolla, 1996.

E. P. Dever, M. C. Hendershott, and C. D. Winant, Center for Coastal Studies -0209, Scripps Institution of Oceanography, University of California, San Diego, 9500 Gilman Drive, La Jolla, CA 92093-0209. (e-mail: edever@ucsd.edu)

(Received October 7, 1997; revised June 3, 1998; accepted June 29, 1998.)